Journal of Biomedical Optics

SPIEDigitalLibrary.org/jbo

New pediatric vision screener employing polarization-modulated, retinal-birefringence-scanning-based strabismus detection and bull's eye focus detection with an improved target system: opto-mechanical design and operation

Kristina Irsch
Boris I. Gramatikov
Yi-Kai Wu
David L. Guyton

SPIE

New pediatric vision screener employing polarization-modulated, retinal-birefringence-scanning-based strabismus detection and bull's eye focus detection with an improved target system: opto-mechanical design and operation

Kristina Irsch,* Boris I. Gramatikov, Yi-Kai Wu, and David L. Guyton
Johns Hopkins University School of Medicine, Wilmer Eye Institute, 600 North Wolfe Street, Wilmer 233, Baltimore, Maryland 21287

Abstract. Amblyopia ("lazy eye") is a major public health problem, caused by misalignment of the eyes (strabismus) or defocus. If detected early in childhood, there is an excellent response to therapy, yet most children are detected too late to be treated effectively. Commercially available vision screening devices that test for amblyopia's primary causes can detect strabismus only indirectly and inaccurately via assessment of the positions of external light reflections from the cornea, but they cannot detect the anatomical feature of the eyes where fixation actually occurs (the fovea). Our laboratory has been developing technology to detect true foveal fixation, by exploiting the birefringence of the uniquely arranged Henle fibers delineating the fovea using retinal birefringence scanning (RBS), and we recently described a polarization-modulated approach to RBS that enables entirely direct and reliable detection of true foveal fixation, with greatly enhanced signal-to-noise ratio and essentially independent of corneal birefringence (a confounding variable with all polarization-sensitive ophthalmic technology). Here, we describe the design and operation of a new pediatric vision screener that employs polarization-modulated, RBS-based strabismus detection and bull's eye focus detection with an improved target system, and demonstrate the feasibility of this new approach. © *The Authors. Published by SPIE under a Creative Commons Attribution 3.0 Unported License. Distribution or reproduction of this work in whole or in part requires full attribution of the original publication, including its DOI.*
[DOI: 10.1117/1.JBO.19.6.067004]

Keywords: vision screening; polarization-sensitive ophthalmic technology; ophthalmology; eye; retina; cornea; birefringence; polarized light; amblyopia; strabismus.

Paper 140182R received Mar. 19, 2014; revised manuscript received May 15, 2014; accepted for publication May 15, 2014; published online Jun. 9, 2014.

1 Introduction

Amblyopia ("lazy eye"), i.e., poor vision in an otherwise normal eye, is a major public health problem, involving up to 4% of children—more in medically underserved populations—and is also among the three leading causes of visual impairment in adults.[1] Of particular significance is that amblyopia can be successfully treated, but only in early childhood, especially during infancy. Delayed treatment, on the other hand, generally results in lifelong visual morbidity. Unfortunately, most children are detected too late to be treated effectively. There are a number of reasons for this, but the major limitation is that there is at present no widely accepted, easily used, and well-validated device that allows the screening of the primary causes of amblyopia, which are strabismus (a misalignment of the eyes in which only one eye fixates on a target at a time) and blurred vision (defocus), in infants and preverbal children. Specifically, commercially available vision screening devices can detect strabismus only indirectly via highly insensitive analysis of the corneal light reflexes, but they cannot detect true foveal fixation of the eyes.

The fovea is the specialized, most sensitive region of the retina that is aimed at the object of regard during fixation. It is surrounded by a radial pattern of birefringent Henle fibers, fibers that change the polarization state of light that passes through them. Guyton et al.[2] have developed technology for detecting true foveal fixation binocularly, by exploiting the birefringence of the Henle fibers, using retinal birefringence scanning (RBS). In RBS, polarized near-infrared light is directed onto the retina in a circular scan (subtending 3 deg of visual angle), with a fixation point in the center, and the polarization-related changes in light retro-reflected from the ocular fundus are analyzed via differential polarization detection using a dual-photodetector system.[3] Because of the radially symmetric arrangement of the birefringent Henle fibers surrounding the fovea, a characteristic frequency appears in the resulting RBS signal when the scan is centered on the fovea, indicating fixation on the central fixation point. By determining the frequency components in the RBS signal from each eye, using a fast Fourier transform (FFT)[2,3] or other techniques,[4] the goodness of eye alignment, and thus strabismus, can be detected.[5] By combining both RBS-based eye alignment and focus detection[6] in a single hand-held device, the previous version of our pediatric vision screener has shown promise as a screening device for the primary causes of amblyopia.[7–10] In contrast to other photoscreeners, by detecting the projection into space of the Henle fibers delineating the fovea (rather than external features of the eye), our RBS-based method of strabismus detection has been shown to detect even small angles of misalignment.[11]

*Address all correspondence to: Kristina Irsch, E-mail: kirsch1@jhmi.edu

We recently described a polarization-modulated approach to RBS,[12] optimized using an algorithm implemented in MATLAB (Mathworks, Inc., Natick, Massachusetts) and validated in human eyes, that provides unique advantages over conventional RBS; it enables differential retinal-birefringence-based detection of foveal fixation in a single-photodetector arrangement, essentially independently of corneal birefringence (all polarization-sensitive ophthalmic technology is adversely affected by corneal birefringence,[13–19] which contributes most to the overall ocular birefringence and varies widely from one eye to the next[20–22]). The new approach also eliminates most of the background noise associated with conventional RBS,[3,5,7–11,23–25] thereby greatly improving the signal-to-noise ratio (SNR).

In this paper, the design of a new pediatric vision screener that combines polarization-modulated RBS-based strabismus detection with double-pass focus detection using a bull's eye photodetector and improved target system is described in detail, and its performance is demonstrated and tested in two adult volunteers and two pediatric patients.

2 Polarization-Modulated, RBS-Based Strabismus Detection

The polarization-modulated approach to RBS described in Ref. 12 incorporates a double-pass half-wave plate (HWP) spinning 9/16th as fast as the circular scan and a double-pass wave plate having a retardance of 106 deg and a fixed fast axis at an azimuth of 0 deg, both optimized using an algorithm implemented in MATLAB.

Use of the HWP, spinning at a particular fraction of the scan frequency, enables measurement of a differential polarization signal with a single photodetector (single-photodetector RBS approach) per eye. This eases optical fabrication and alignment tolerances as well as simplifies the electronics as compared with conventional dual-photodetector RBS arrangements. In addition, it eliminates the need for a nonpolarizing beam splitter which decreased signal attenuation in the previous versions. A differential polarization signal is calculated digitally via 360 deg phase-shift subtraction. By spinning the HWP 9/16th as fast as the circular scan, strong signals are generated that are half multiples of the scanning frequency. These half-multiple frequency signals double in amplitude and even quadruple in signal strength (FFT power) with 360 deg phase-shift subtraction, whereas most of the optical background noise, at whole multiples of the scanning frequency, is eliminated, thus greatly increasing the SNR in RBS.

The addition of a 106 deg double-pass wave plate at a fixed fast axis azimuth of 0 deg yields high and uniform differential RBS signals across the entire known population range of corneal retardances and azimuths, allowing differential polarization detection essentially independent of corneal birefringence.

With central fixation, two frequency components predominate the RBS signal, that is, 6.5 times the scanning frequency ($6.5f$, predominant for the majority of people, who have eyes with lower relative corneal retardance) and 2.5 times the scanning frequency ($2.5f$, predominant for a minority of people, who have eyes with higher relative corneal retardance), whereas with paracentral fixation, with the scan no longer centered on the fovea, signal strength (FFT power) at these frequencies falls off (with other frequency components, $5.5f$ and $3.5f$, occurring in the signal), so that the presence and/or absence, of these various frequency components distinguishes between central and paracentral fixation. Thus, spectral analysis using FFT (for each eye) allows assessment of each eye's fixation condition, and thus detects either proper alignment or strabismus.

In addition to the specific half-multiple frequencies indicating central fixation ($2.5f$ and $6.5f$), another half-multiple frequency component ($4.5f$) occurs in the RBS signal at a frequency that is determined by the HWP rotation speed (resulting here in a $4.5f$ "spin-generated frequency"). This spin-generated frequency is present whenever the HWP is present and is spinning, with an amplitude practically independent of the eye's fixation condition and present both during central and paracentral fixation. With addition of the 106 deg wave plate (at fast axis azimuth 0 deg), the amplitude of the spin-generated frequency also becomes essentially independent of corneal birefringence. The spin-generated frequency can thus be used to great advantage for normalization purposes, which is necessary to compensate for variations in fundus reflectivity, pupil sizes, light levels, and dust that gathers on the optics over time.

3 Bull's Eye Focus Detection

Bull's eye focus detection has been described elsewhere in detail,[2,6] and is accomplished by using a bull's-eye photodetector for differential detection of the goodness of focus of the retro-reflected light from the retinal birefringence scan. Briefly, fundus-reflected near-infrared light is focused by the optical system of the eye onto a bull's eye photodetector, optically conjugate to the fixation target, and consisting of two concentric active areas, a circular center (C) with a surrounding annulus (A), each with essentially the same total area. When the eye is in good focus, most returning light is imaged onto C, and $C \gg A$. When the eye is partially or fully out of focus, the amount of light received by the annulus increases, with $C \approx A$ for complete defocus. Thus, the goodness of focus that an eye is experiencing can be determined by the ratio of the detected center to annulus signals, more precisely by the normalized ratio $(C - A)/(C + A)$, which will also compensate for variations in fundus reflectivity.

Because the $4.5f$ spin-generated frequency component is a strong signal and is essentially independent of both corneal birefringence and the fixation condition of the eye, it is nicely suited not only for normalization purposes of the RBS signal but also for independent assessment of the state of focus.

4 Instrument Design and Operation

In the new pediatric vision screener (PVS), polarization-modulated RBS has been combined with bull's eye focus detection, binocularly, to allow simultaneous assessment of strabismus and defocus. In anticipation that the instrument will be used as a strabismus/defocus screening tool for infants and children at risk for amblyopia, additional design constraints were identified as follows. To allow remote assessment, the device had to be hand-held and portable enough so that it could be aimed at children seated on a parent's lap without head restraint, and it had to have the ability to attract the child's attention.

4.1 *Optical and Mechanical Design*

Figure 1 illustrates the optical component layout and light paths of the new PVS. Linearly polarized light emitted continuously by the main 785-nm laser diode (LD1) passes through a pair of plano-convex lenses (LP1), and is then transmitted by a plate polarizing beam splitter (PBS) toward an HWP that is spun by a motor using a pulley ratio to achieve a rotation 9/16th

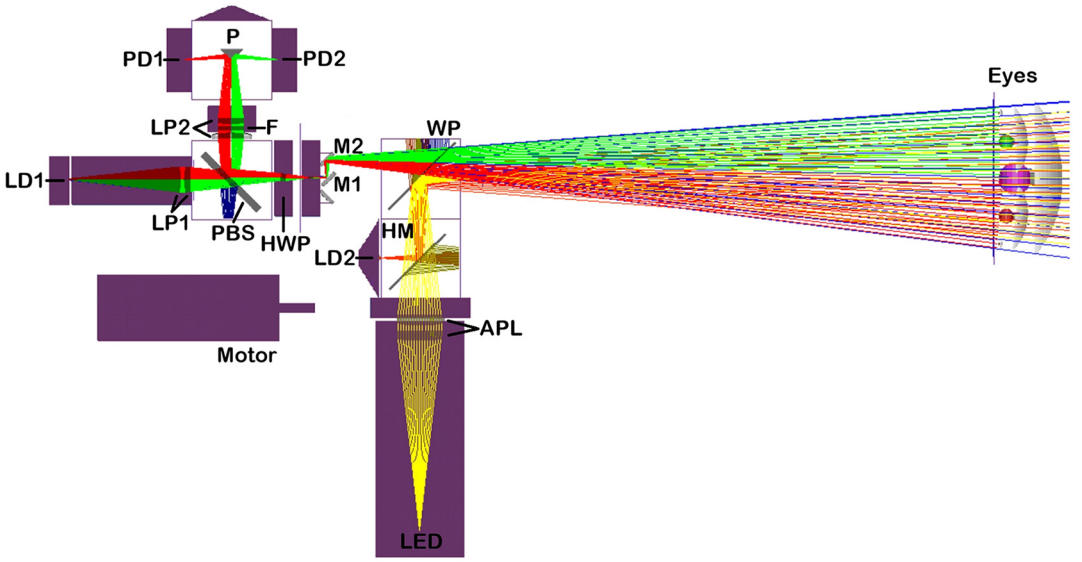

Fig. 1 Ray tracing diagram and physical layout of the new pediatric vision screener.

as fast as the scan (explained below). After passage through the rotating HWP, the beam of continuously rotating linearly polarized light enters the scanning unit that consists of two gold-plated plane mirrors (M1 and M2). The scanning unit is driven by the same motor, thus turning the stationary beam of light into a circular scan. Light from the outer scanning mirror (M2) travels toward the eyes through a 106 deg retarder (WP) with its fast axis oriented horizontally (0 deg azimuth). While each eye is fixating, or focusing, on a blinking red light generated by a 690-nm laser diode (LD2), optically conjugate to, and appearing to be in, the very center of the scanning circle, each retina is scanned by the spot of laser light in a circle subtending a visual angle of 3 deg in diameter. The small percentage of light reflected from each ocular fundus is reimaged back, following the same light path it originally came from, via the principle of conjugacy. The unchanged part of the returning light, in other words the part with the same polarization as the original plane of polarization, is transmitted through the PBS back toward the light source, thus never making it to the detection unit. The changed part of the returning light, on the other hand, is reflected by the PBS toward the photodetector assembly, consisting of two bull's-eye photodetectors (PD1 and PD2), one for each eye. Note that the eyes and photodetector assembly have been rotated 90 deg about the optical axis for clarity of illustration. A band pass filter (F) ensures that only light in the desired wavelength range reaches the detectors. It is positioned between another pair of plano-convex lenses (LP2) to avoid shifting of the filter's peak transmission to a shorter wavelength, which can occur if used in convergent or divergent light. The lens pair images the spatially preserved signals from the right and left eyes, separated by a knife-edge reflecting prism (P) conjugate to the plane of the pupils, toward PD1 and PD2.

As with previous designs, the fixation target is a red light in the center of the scanning circle, which is flashing on and off to attract the child's attention. The fixation light is produced by the 690-nm laser diode (LD2) positioned physically conjugate to the plane of the main 785-nm laser (LD1). However, as eyes do not accommodate (focus) well on monochromatic light,[26] we now employ an improved target system with accommodative control. Specifically, a black-and-white grid printed on a transparency serves as an accommodative target, which is illuminated by a white-light LED array. This white-light accommodative background is imaged 1:1 by an achromatic lens pair (APL) into an aerial image plane that is 33 cm away from the subject, a standard near testing distance for children. Greater distances in general cause young subjects to lose interest in the target. To account for the eye's longitudinal chromatic aberration, the image of the RBS spot of 785-nm light is located 0.75 D farther away than the 33-cm distance of the accommodative grid target, at 44.4 cm. Thus, with an eye fixating on the blinking 690-nm light, with focus controlled by the black-and-white background at 33 cm, the near-infrared light from the scanning 785-nm laser diode will be in proper focus on the retina.

Figure 2 illustrates the mechanical component layout of the new PVS. To run the HWP at a fractional frequency of the scan (9/16 times as fast), a special timing-belt-drive system is used that transmits different speeds to the HWP (mounted within the left-hand pulley) and to the scanning unit (the black plastic disk attached to the right-hand pulley). To achieve the 9:16 rotation ratio of the HWP to the scanning unit, the implemented belt drive system uses a pulley with 18 teeth to drive the HWP and a pulley with 32 teeth to drive the scanning unit. The resulting ratio of 18 to 32 equals 9:16 as required.

4.2 *Signal Acquisition and Analysis: Strabismus Detection and Focus Detection*

Signals from the bull's-eye photodetectors (center and annulus for each eye) are amplified and filtered, and then fed to a computer for analog-to-digital conversion and analysis. The main signal analysis procedure is the FFT (using the power spectrum). The concept of both alignment and focus detection using a single bull's-eye photodetector (per eye) is detailed in the following section.

For each eye, during central fixation (on the blinking target presented in the center of the scanned circle) and thus with the scanned circle of polarized near-infrared (785 nm) light centered on the fovea, the signal of the returning light has a strong frequency component that is 6.5 times and/or 2.5 times the scanning frequency. The $6.5f$ signal is predominant for the majority

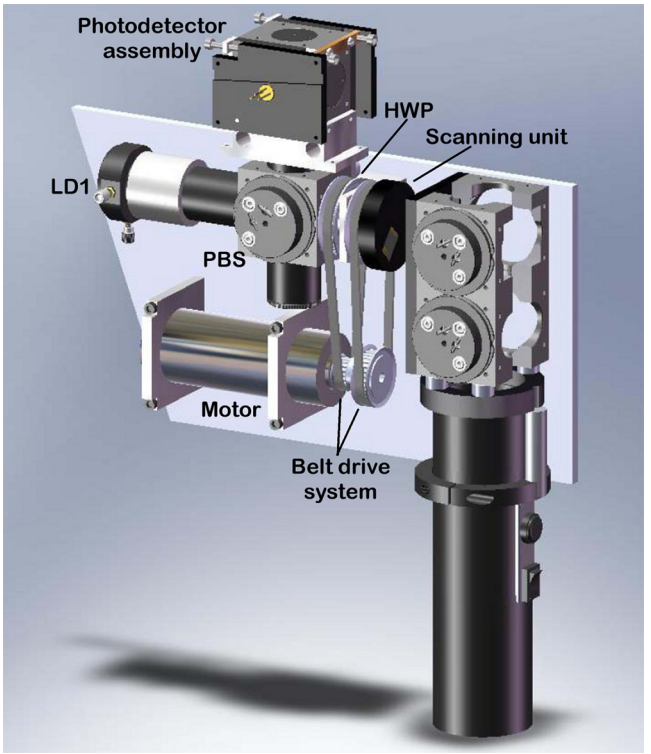

Fig. 2 Mechanical component layout of the new pediatric vision screener.

of people, who have eyes with lower relative corneal retardance, whereas the $2.5f$ signal is predominant for the minority of people, who have eyes with higher relative corneal retardance. The returning light also has a strong frequency component that is 4.5 times the scanning frequency (the spin-generated frequency), that is independent of the fixation condition and essentially independent of the corneal birefringence of each eye. For the new PVS, the frequency of the scan (f) is 30 Hz, so that a predominant 195-Hz ($6.5f$) or 75-Hz ($2.5f$) component in the signal indicates central fixation. Thus, spectral analysis, using FFT for each eye, reveals whether a subject is fixating on the target with one eye (as is the case with strabismus), both eyes (no strabismus), or neither eye (inattention). More precisely, the fixation condition of each eye is assessed by computing the FFT power spectrum of the signal from that eye's central detector and assessing the combined powers at 75 and 195 Hz, normalized by the power at 135 Hz $[(P_{2.5f} + P_{6.5f})/P_{4.5f}]$, which compensates for variations in fundus reflectivity.[12]

Thirty scan cycles are acquired to obtain the differential polarization signal, which is calculated by digitally shifting the signal by one scanning period (360 deg) and subsequently subtracting it from the original signal (360 deg phase-shift subtraction). The FFT power spectrum is computed on the resultant 29-cycle differential signal.

Although the state of fixation of each eye is a function of which frequencies dominate the overall signal, the state of focus of an eye is dependent on the amount of light hitting the central versus annular active areas of the bull's-eye detector. If the eye is in good focus on the accommodative background target at 33 cm, most of the returning 785-nm light will fall on the central detector, but if it is out of focus, light will fall on both the center and annulus detectors.

The spin-generated frequency $4.5f$ (135 Hz), being essentially independent of corneal birefringence and especially independent of the fixation condition, is also nicely suited for independent assessment of the state of focus. The goodness of focus of each eye is assessed by first computing the

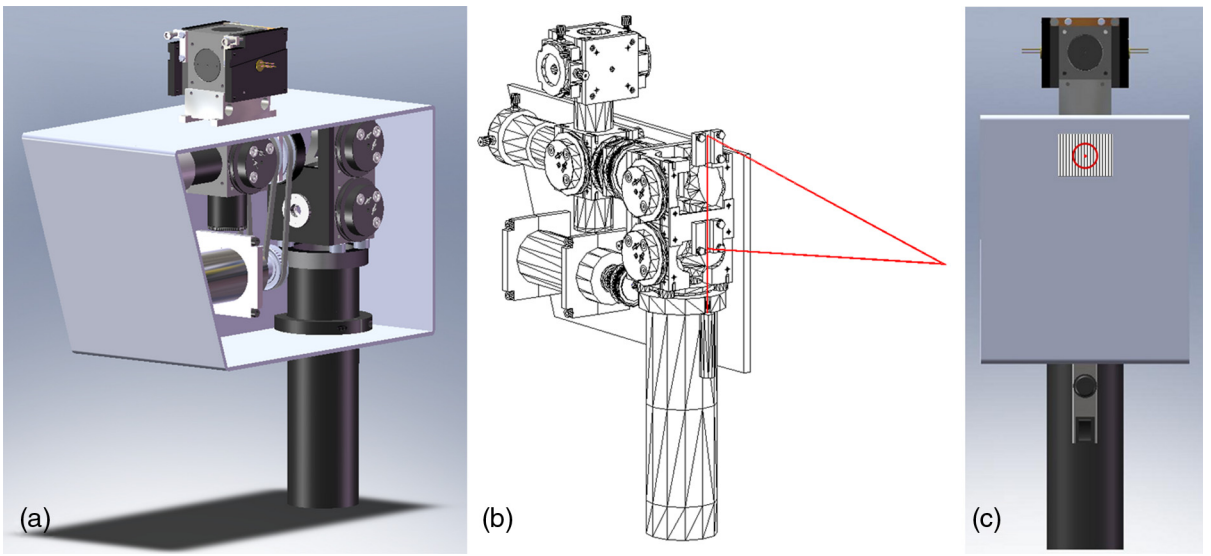

Fig. 3 Mechanical model of the new pediatric vision screener in operation. (a) Oblique view of entire device from operator's side helping to show mechanical component layout. Note the hand-held configuration of the device and (b) the triangulation range finder that enables remote examination. The infant can be seated on a parent's lap, for instance, while the operator aims the screener with the help of the laser pointer range finder. Axial distance is correct when the two laser spots overlap on the bridge of the child's nose. Once aligned, the operator presses a button to activate the measurement. (c) Child's view of white-light grid for accommodation control, with blinking fixation target in the center, surrounded by faint scanning circle.

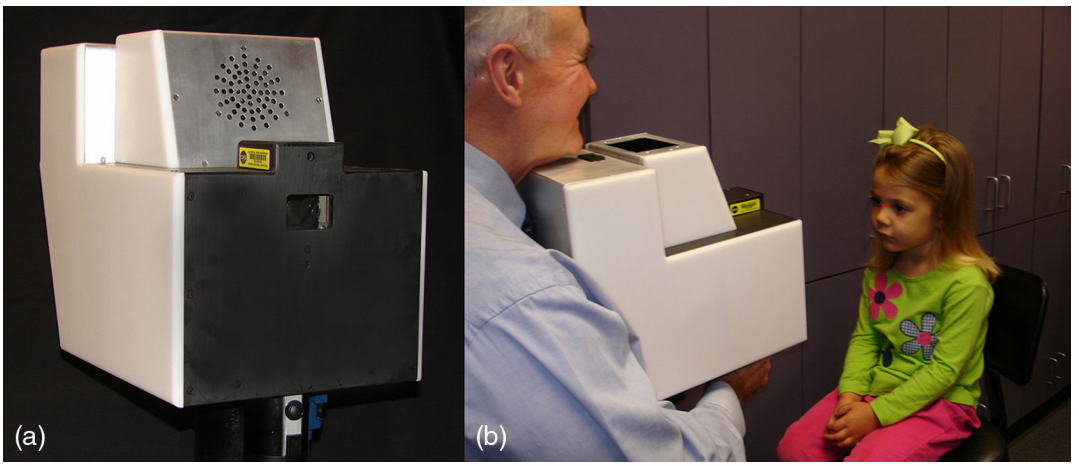

Fig. 4 The pediatric vision screener in operation. (a) Device mounted on a stand for ease of performance evaluation in adults. (b) Remote examination of a child seated on a chair while the operator aims the device. Note that the two laser spots overlapping on the bridge of the child's nose indicating proper viewing alignment.

power spectrum of both the center (C) (already done as part of the fixation condition assessment of each eye) and annulus (A) signals, and then assessing the FFT powers at 135 Hz in the center and annulus signals via their normalized difference $[(C-A)/(C+A)]$, which produces a predictable range from 0 to 1 for a completely defocused and perfectly focused eye, respectively.

4.3 *Device Operation*

The device in operation is illustrated in Figs. 3 and 4. The handheld configuration of the instrument allows remote examination of a child without head restraint. The child can be seated on a chair or in the parent's lap, while the operator aims and activates the instrument. A low-power laser diode range finder enables quick and easy adjustment of the proper target viewing distance of 33 cm [see Fig. 3(b)]. This desired axial distance (not critical) is achieved when the two laser spots overlap on the bridge of the child's nose [see Fig. 4(b)]. During the exam, the child sees the blinking light within the aperture of the apparatus [see Fig. 3(c)]. The flashing fixation target is presented in combination with a tone to encourage the child to maintain fixation on the flashing light. Room lights are dimmed to further enhance interest in the target, as well as to aid pupil dilation to increase the amount of light entering the eyes. For initial performance evaluation in adult volunteers (see Sec. 5), the device was mounted on a stand for ease of testing [see Fig. 4(a)].

The operator can initiate data acquisition by simply pushing the upper trigger button at the front of the handle [see Fig. 3(c)]. Software was written (B.I.G.) in C language (CVI, National Instruments, Austin, Texas) and includes a graphical user interface. To assess the goodness of eye alignment, the FFT power spectrum of the central detector (C) is displayed as separate plots for the right and left eyes (see upper two plots in Fig. 5). For the additional information needed for focus assessment, additional plots showing the FFT power spectrum of the annulus (A) are displayed for the right and left eyes (see lower plots in Fig. 5), allowing assessment of the power of interest at 135 Hz ($4.5f$) in both center and annulus signals.

In anticipation that the PVS will be used as a screening tool administered by lay personnel, the device will additionally display the findings in the form of pass/refer(fail) indicator lights on the outer case of the device facing the operator (similar to Ref. 8).

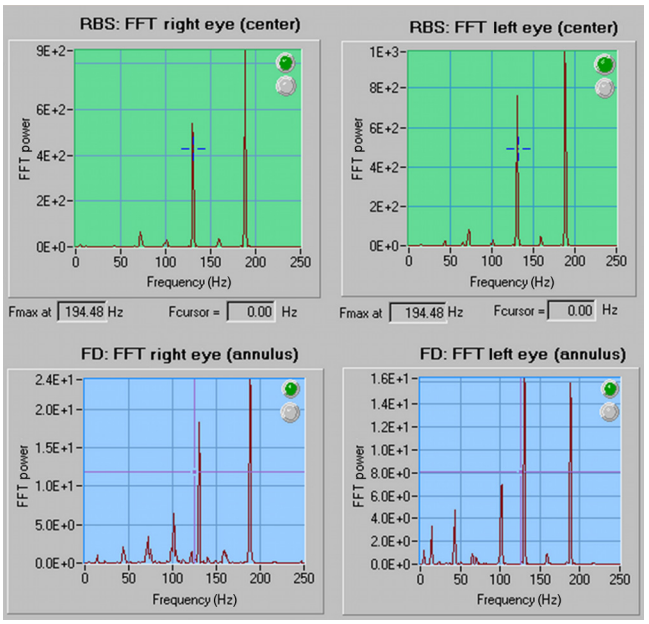

Fig. 5 FFT power spectra of the central detector (upper two plots) and annulus (lower two plots) are displayed for the right and left eyes, allowing assessment of both strabismus and focus. Upper light within each plot indicates passing measurement. In this case, the subject demonstrated bilateral foveal fixation (eye alignment) and bilateral focus.

5 Performance Testing

Although the performance of binocular polarization-modulated, RBS-based fixation detection has already been demonstrated in adult volunteers,[12] we wished to specifically test the performance of bull's eye focus detection with the improved target system, and also to assess the feasibility of the new PVS in testing less cooperative children and identifying their fixation/focus abnormalities.

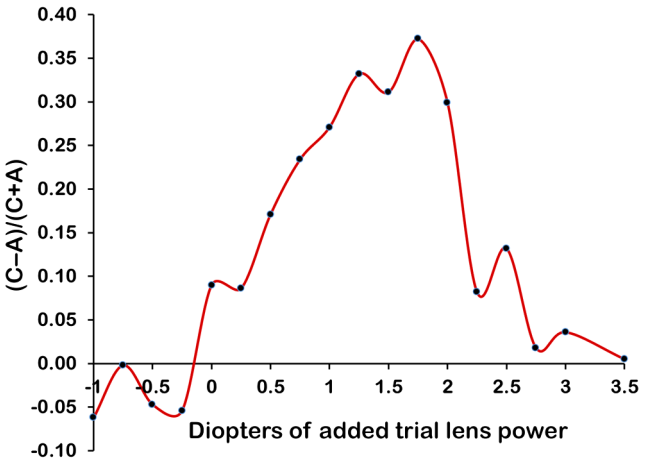

Fig. 6 Focus curve with a presbyopic eye (age 67), stepping through best focus in 0.25 D increments. Each point represents the average of 10 1-s epochs of data collection. Note that the width of the focus curve at half maximum (FWHM) is approximately ±1.00 D.

The investigations were approved by the Johns Hopkins University Institutional Review Board and adhered to the tenets of the Declaration of Helsinki. Prior to the investigations, informed consent was obtained from either the subject or the parent after the nature and possible consequences of the study were explained, and a "gold standard" clinical evaluation was performed by an ophthalmologist (D.L.G.) to assess the subject's ocular condition.

First, two adult volunteers, including a 29-year-old individual with emmetropic eyes (no refractive error) and a 67-year-old presbyopic individual with myopic eyes and essentially no remaining focusing ability were studied (as in Ref. 12) to assess the potential of the new PVS in detecting focus. Ophthalmic trial lenses, tilted to avoid reflections, were placed in front of the subject's eye to simulate various refractive errors. Trial lenses were selected to step through the point of best focus in 0.25 D increments. Focus curves were generated by plotting the normalized differences $(C-A)/(C+A)$ at 135 Hz measured with each trial lens. To specifically test the performance of the improved target system with white-light accommodative control, for the nonpresbyopic (accommodating) subject, focus curves were determined with the white-light grid turned on, and then off.

With resulting preliminary threshold settings from these and previous[12] performance evaluations in adult volunteers, we then assessed the feasibility of the new PVS in identifying strabismus/defocus in two children, including a 9-year-old child with amblyopia and small-angle (3 prism diopters) of left eye esotropia (turning in of the left eye), and a 3-year-old child with reasonably high hyperopia (+4.75 D) in both eyes and accommodative right eye esotropia (turning in of the right eye only when focusing intently on a near target).

6 Results

The focus curve obtained with the presbyopic, nonaccommodating subject's right eye is shown in Fig. 6. The curve's peak is located at approximately +1.50 D (where the grid appeared to be in best focus according to the observations of the subject) with a full width at half maximum (FWHM) of about ±1 D, the design goal at this stage.

Figure 7 shows the focus curves of the nonpresbyopic, accommodating subject's right eye, obtained with the white-light grid turned (a) on and (b) off. The subject reported that, with the minus lenses, it was easier to hold focus on the red ring and central fixation spot when the white-light background grid was turned on, consistent with the curve falling off more quickly, especially in the minus lens direction, when the white-light grid was turned off [see Fig. 7(b)].

Figures 8 and 9 demonstrate the feasibility of testing less cooperative children and identifying their fixation/focus abnormalities. The 9-year-old child with amblyopia and small angle of left eye esotropia (3 prism diopters; 1.7 deg) is shown in Fig. 8. As expected, central fixation is detected only in the right eye (as indicated by illumination of the upper light in the upper right-hand corner), whereas the other, misaligned eye correctly shows misalignment with illumination of the lower indicator light, confirming the device's capability of detecting even small deviations.[12] Figure 9 illustrates the potential of the new PVS in detecting the misalignment in patients with accommodative esotropia who only develop a crossed

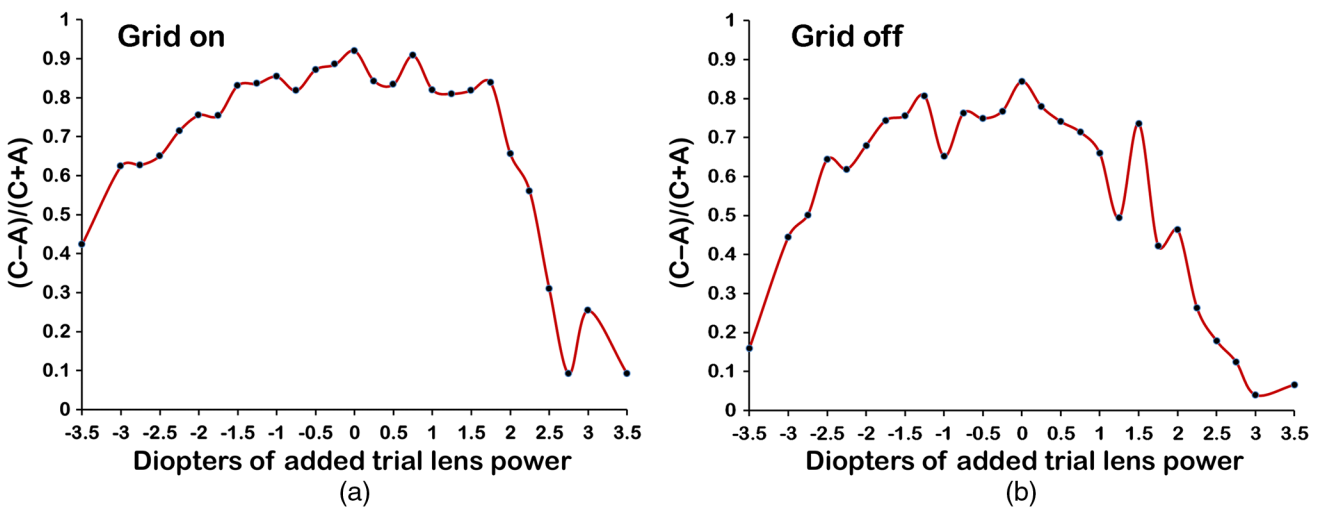

Fig. 7 Focus curve from a nonpresbyopic, accommodating eye (age 29), obtained with white-light grid turned (a) on and (b) off. Note that the focus curve falls off more quickly, especially in the minus lens direction, with the white-light grid turned off.

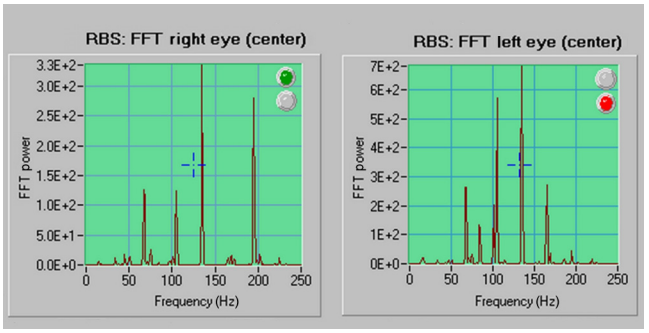

Fig. 8 FFT power spectra (from the central detector) from a 9-year-old child with amblyopia and a small angle (3 prism diopters) of left eye esotropia, showing central fixation by the right eye (upper indicator light illuminated) and misalignment of the left eye (lower indicator light illuminated).

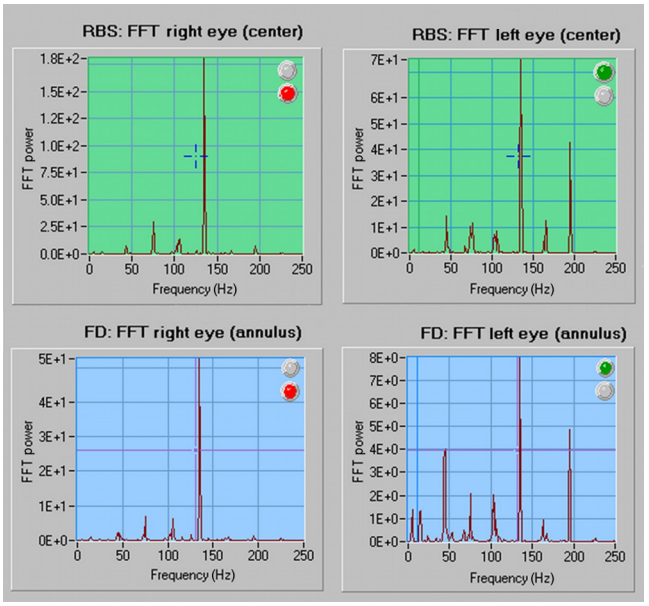

Fig. 9 FFT power spectra from a 3-year-old child with reasonably high uncorrected bilateral hyperopia (+4.75 D) and accommodative right eye esotropia, showing central fixation in the fixing left eye (upper indicator light illuminated in upper right plot) and misalignment of the nonfixing right eye (lower indicator light illuminated in the upper left plot), as the child accommodates to overcome the hyperopia, and her right eye turns inward.

eye when focusing intently on a near target. Results from the 3-year-old child are shown as she accommodates on the white-light background with her left eye while fixing properly on the blinking central light, as indicated by illumination of the upper indicator light in the lower right plot. Accommodating enough to overcome her reasonably high hyperopia, however, results in crossing of the nonfixing, right eye (as indicated by illumination of the lower indicator light in the upper left plot).

7 Discussion and Conclusion

The new pediatric vision screener described in this paper uses polarization-modulated RBS for strabismus detection, and a bull's eye photodetector conjugate to the light source for double-pass focus detection with an improved target system.

The accommodation control with the improved target system, and the use of the plane-mirror scanning system that avoids optical aberrations in the double-pass system introduced by the concave mirror in earlier designs,[8] enable the double-pass image of the RBS spot of light to be used simultaneously for alignment assessment and focus detection using the bull's-eye focus detector. This significantly simplifies the combination of both technologies in the new PVS. Also, the incorporation of the spinning HWP, which allows differential polarization detection with a single detector (single-photodetector RBS system) per eye instead of two (dual-photodetector RBS system), significantly reduces the overall number of detectors to just one bull's-eye detector per eye, and eliminates the need for additional beam splitters in the optical pathway that attenuate the signal. In contrast, the previous version of our PVS required six detectors in total,[8] four for detection of the differential foveal fixation signals (one dual-photodetector system for each eye), and two bull's-eye detectors for focus detection.

Moreover, although our RBS-based method of foveal fixation detection requires no eye-gaze calibration, the previous version of our PVS (Ref. 8) required a preliminary background measurement for each subject with eyes closed, which was then subtracted from subsequent measurements with eyes open to improve the SNR. Our polarization-modulated approach to RBS has eliminated most of the background noise associated with conventional RBS,[12] so that no additional eyes-closed background measurement is required with the new PVS.

By detecting the projection into space of the Henle fibers delineating the fovea (rather than external features of the eye, as is the case with current photoscreeners), our approach of strabismus detection is capable of detecting even small angles of eye misalignment (at least 0.75 deg or 1.3 prism diopters[12]), as illustrated in our feasibility study in children.

Feasibility tests of focus detection with our new PVS using the improved target system with accommodation control suggest that the device has the potential to detect spherical focus within ± 1.00 D, based on the focus curve's FWHM of approximately ± 1.00 D in our presbyopic subject. The white-light grid appeared to help stimulate and hold accommodation at 33 cm, with the focus curve of a nonpresbyopic, accommodating eye falling off sooner with the grid turned off. The subject also reported that it was hard to hold focus on the ring and central fixation spot when the white-light accommodative grid was turned off, as had been the case with earlier versions of our PVS.[8] As demonstrated in our 3-year-old child, our improved white-light grid target system that stimulates proper accommodation should aid in detecting the misalignment in patients with accommodative esotropia who only develop a crossed eye when focusing intently on a near target.

In conclusion, the new PVS shows real promise in supplying the demand for a reliable, automated strabismus/defocus screening tool for infants and children at risk for amblyopia. We have started pilot testing the device with well-characterized strabismic/anisometropic subjects (or those having other "defocus" conditions) and healthy controls to fine-tune threshold settings for pass/fail signal levels. Future studies with finalized threshold settings, followed by independent clinical trials involving a large number of pediatric patients, will determine the full potential of the device.

Acknowledgments

This work was supported in part by gifts from Robert and Maureen Feduniak, Dewey and Janet Gargiulo, David and Helen Leighton, Richard and Victoria Baks, Robert and

Diane Levy, and by awards from the Hartwell Foundation (B. I. G., K. I.), Research to Prevent Blindness (D. L. G.), and the Knights Templar Eye Foundation (K. I.).

References

1. K. Simons, "Amblyopia characterization, treatment, and prophylaxis," *Surv. Ophthalmol.* **50**(2), 123–166 (2005).
2. D. L. Guyton et al., "Eye fixation monitor and tracker," U.S. Patent No. 6,027,216 (2000).
3. D. G. Hunter, S. N. Patel, and D. L. Guyton, "Automated detection of foveal fixation by use of retinal birefringence scanning," *Appl. Opt.* **38** (7), 1273–1279 (1999).
4. B. I. Gramatikov, "Detecting fixation on a target using time-frequency distributions of a retinal birefringence scanning signal," *Biomed. Eng. Online* **12**, 41 (2013).
5. D. G. Hunter et al., "Automated detection of ocular alignment with binocular retinal birefringence scanning," *Appl. Opt.* **42**(16), 3047–3053 (2003).
6. D. G. Hunter et al., "Automated detection of ocular focus," *J. Biomed. Opt.* **9**(5), 1103–1109 (2004).
7. D. S. Nassif et al., "Pediatric vision screening using binocular retinal birefringence scanning," *Proc. SPIE* **4951**, 9–20 (2003).
8. D. G. Hunter et al., "Pediatric Vision Screener 1: instrument design and operation," *J. Biomed. Opt.* **9**(6), 1363–1368 (2004).
9. D. S. Nassif et al., "The Pediatric Vision Screener II: pilot study in adults," *J. Biomed. Opt.* **9**(6), 1369–1374 (2004).
10. D. S. Nassif, N. V. Piskun, and D. G. Hunter, "The Pediatric Vision Screener III: detection of strabismus in children," *Arch. Ophthalmol.* **124**(4), 509–513 (2006).
11. S. E. Loudon et al., "Rapid, high-accuracy detection of strabismus and amblyopia using the pediatric vision scanner," *Invest. Ophthalmol. Vis. Sci.* **52**(8), 5043–5048 (2011).
12. K. Irsch et al., "Improved eye-fixation detection using polarization-modulated retinal birefringence scanning, immune to corneal birefringence," *Opt. Express* **22**(7), 7972–7988 (2014).
13. K. Irsch et al., "Modeling and minimizing interference from corneal birefringence in retinal birefringence scanning for foveal fixation detection," *Biomed. Opt. Express* **2**(7), 1955–1968 (2011).
14. M. Pircher et al., "Corneal birefringence compensation for polarization sensitive optical coherence tomography of the human retina," *J. Biomed. Opt.* **12**(4), 41210 (2007).
15. Q. Zhou and R. N. Weinreb, "Individualized compensation of anterior segment birefringence during scanning laser polarimetry," *Invest. Ophthalmol. Vis. Sci.* **43**(7), 2221–2228 (2002).
16. Q. Zhou, "System and method for determining birefringence of anterior segment of the patient's eye," U.S. Patent No. 6,356,036 (2002).
17. Q. Zhou, "Retinal scanning laser polarimetry and methods to compensate for corneal birefringence," *Bull. Soc. Belge Ophtalmol.* **302**, 89–106 (2006).
18. N. J. Reus, Q. Zhou, and H. G. Lemij, "Enhanced imaging algorithm for scanning laser polarimetry with variable corneal compensation," *Invest. Ophthalmol. Vis. Sci.* **47**(9), 3870–3877 (2006).
19. B. H. Malik and G. L. Coté, "Modeling the corneal birefringence of the eye toward the development of a polarimetric glucose sensor," *J. Biomed. Opt.* **15**(3), 37012 (2010).
20. R. W. Knighton and X. R. Huang, "Linear birefringence of the central human cornea," *Invest. Ophthalmol. Vis. Sci.* **43**(1), 82–86 (2002).
21. R. N. Weinreb et al., "Measurement of the magnitude and axis of corneal polarization with scanning laser polarimetry," *Arch. Ophthalmol.* **120**(7), 901–906 (2002).
22. K. Irsch and A. A. Shah, "Birefringence of the central cornea in children assessed with scanning laser polarimetry," *J. Biomed. Opt.* **17**(8), 086001 (2012).
23. B. I. Gramatikov et al., "Birefringence-based eye fixation monitor with no moving parts," *J. Biomed. Opt.* **11**(3), 034025 (2006).
24. B. I. Gramatikov et al., "Directional eye fixation sensor using birefringence-based foveal detection," *Appl. Opt.* **46**(10), 1809–1818 (2007).
25. B. Gramatikov et al., "A device for continuous monitoring of true central fixation based on foveal birefringence," *Ann. Biomed. Eng.* **41**(9), 1968–1978 (2013).
26. K. R. Aggarwala, S. Nowbotsing, and P. B. Kruger, "Accommodation to monochromatic and white-light targets," *Invest. Ophthalmol. Vis. Sci.* **36**(13), 2695–2705 (1995).

Biographies of the authors are not available.